MINERALOGICAL MAGAZINE

VOLUME 58 NUMBER 390 MARCH 1994

Triple-chain pyriboles in Lewisian ultramafic rocks

G. T. R. DROOP

Department of Geology, University of Manchester, Manchester M13 9PL, U.K.

Abstract

The triple-chain pyriboles jimthompsonite, clinojimthompsonite, and probably chesterite and its monoclinic polytype occur in Lewisian amphibolite-facies ultramafic rocks near Achmelvich, N.W. Scotland. These minerals are intergrown with one another and with amphiboles in prismatic porphyroblasts up to 3 cm long, which are associated with chlorite, carbonate, magnetite and, in some cases, talc. Rocks containing triple-chain silicates have been found at three localities, in each case outcropping in a layer < 1.5 m thick. Clinojimthompsonite is the most abundant triple-chain silicate and generally forms euhedral wedge-shaped overgrowths, measuring up to 1 mm in the *b*-axis direction, on the {010} faces of actinolite cores. The mineral assemblages are probably of Inverian age.

The identification of the triple-chain phases is based mainly on cleavage angle, extinction angle, back-scattered electron intensity and, in the case of clinojimthompsonite, on X-ray diffraction data. Microprobe analyses support the identifications. The triple-chain silicates have compositions lying in the system MgO–FeO–SiO_2–H_2O, with only trace amounts of other components.

The cell dimensions of the coarsest clinojimthompsonite are: $a = 9.862 \pm 0.002$ Å, $b = 27.184 \pm 0.020$ Å, $c = 5.298 \pm 0.004$ Å, $\beta = 109.61° \pm 0.14°$, $V = 1337.9 \pm 1.8$ Å^3, and its optical properties are as follows: $\alpha = 1.600$ $\beta = 1.619$ $\gamma = 1.628$ (all ± 0.001) and optic axial plane = (010). The $2V_\alpha$ of clinojimthompsonite = $67 \pm 2°$.

Back-scattered electron microscopy reveals that although substantial volumes of single-phase clinojimthompsonite are common, (010) intergrowths of Mg,Fe-amphiboles, jimthompsonite polytypes and chesterite polytypes occur locally on scales down to 0.1 μm and probably smaller, indicating considerable chain-width disorder.

The triple-chain pyriboles are not pseudomorphous after amphibole and probably grew during prograde Inverian metamorphism. Chemographic constraints suggest that they could have formed from forsterite-bearing assemblages, possibly as the result of infiltration of CO_2-rich fluid. Thermodynamic calculations for associated high-variance ultramafic rocks place an upper limit of *c.* 600–700°C on the temperature of metamorphism.

The large number of chemically similar pyriboles and their disposition within compound prisms suggests that crystallization was kinetically controlled. A simple 'template' model is proposed to explain the observed patterns, in which the identity of the Mg,Fe-pyribole nucleating at any point on a pre-existing actinolite or Mg,Fe-pyribole substrate is controlled by silicate-chain width and/or symmetry (ortho *vs.* clino), depending on the orientation of the substrate crystal face.

KEYWORDS: pyriboles, triple-chain silicates, clinojimthompsonite, jimthompsonite, BSEM, nucleation kinetics

Mineralogical Magazine, March 1994, Vol. 58, pp. 1–20

Introduction

MINERALS that belong to the 'biopyribole' polysomatic series may be regarded as having crystal structures composed of talc-like and pyroxene-like (010) layer modules combined in specific proportions (Thompson, 1970, 1978). In amphiboles, for example, the talc-like layers (M) and pyroxene-like layers (P) are present in the ratio 1:1 and alternate regularly (MP repeat pattern), giving rise to the characteristic double chains of SiO_4 tetrahedra. The insertion of extra talc-like layer modules gives rise to structures with wider silicate chains. This paper is concerned primarily with biopyriboles that contain triple silicate chains. Biopyriboles other than micas and talc are known as 'pyriboles'.

Natural triple-chain pyriboles were first described from the blackwall zone of a metamorphosed ultramafic body at Chester, Vermont (Veblen and Burnham, 1975, 1976, 1978*a*, 1978*b*; Veblen and Buseck, 1979, 1980), where they occur as lamellar intergrowths with anthophyllite and cummingtonite in large prismatic crystals. Four pyriboles with compositions intermediate between talc and anthopyllite were originally characterized from this locality: (1) jimthompsonite, an orthorhombic pyribole of idealized composition $(Mg,Fe)_{10}Si_{12}O_{32}(OH)_4$ with triple silicate chains (MMP repeat pattern), (2) clinojimthompsonite, its monoclinic polytype, (3) chesterite, an orthorhombic phase of idealized composition $(Mg,Fe)_{17}Si_{20}O_{54}(OH)_6$ with alternating double and triple chains (MMPMP repeat pattern), and (4) the monoclinic polytype of chesterite, as yet unnamed.

Since the discovery of triple-chain pyriboles (hereafter TCPs) high-resolution transmission electron microscopy has revealed several other occurrences, mostly on a micrometre to nanometre scale. One characteristic type of occurrence is as alteration products of amphiboles or pyroxenes in retrograded or metasomatized rocks. Nissen *et al.* (1979) described small domains of jimthompsonite in hydrothermally altered ultramafic rocks. Lamellae of monoclinic TCP in altered augite have been documented by Nakajima and Ribbe (1980), Veblen and Buseck (1981) and Akai (1982). Livi and Veblen (1992) report mixed double- and triple-chain silicates in altered Mn-rich pyroxenes and pyroxenoids. TCP phases also occur as lamellae and planar defects within primary amphibole crystals. Euhedral prisms of intergrown actinolite and Ca-pyribole have been reported by Yau and Peacor (1985) from hydrothermally metamorphosed sediments. Chesterite-like lamellae (Cressey *et al.*, 1981) and triple-chain defects (Treloar and Putnis, 1982) have been found in anthophyllite, and wide-chain lamellae have been found in fibrous grunerite (Whittaker *et al.*, 1981) and Zn-tremolite (Dorling and Zussman, 1984). Apart from the type material from Chester, however, the only other documented occurrence of relatively coarse-grained TCP, to the author's knowledge, is an amphibolite-facies pyribole-phlogopite-spinel rock from Orijärvi, Finland, which contains prisms of intergrown jimthompsonite, chesterite and anthophyllite (Schumacher and Czank, 1987). Synthetic TCPs have been reported by Drits *et al.* (1974), Tateyama *et al.* (1978), Ahn *et al.* (1991), and Welch *et al.* (1992).

This paper describes an occurrence of TCP in the Lewisian Gneiss of N.W. Scotland. As with the type material, the TCP is hosted by amphibolite-facies ultramafic rocks. Unlike the type material, clinojimthompsonite dominates the association and forms large, volumetrically abundant, euhedral crystal overgrowths that do not appear to be of retrogressive origin.

Occurrence and associations

The Lewisian TCPs occur within a 0.1 km^2 ultramafic/mafic complex which outcrops S.W. of Achmelvich in the vicinity of An Fharaid Mhor, within the National Grid square NC 05 24. The complex comprises a folded sequence of interlayered ultramafic, mafic and quartzo-feldspathic gneisses (Tarney, 1978). The ultramafic rocks, which account for about half of the outcrop, consist mainly of combinations of Ca-amphibole (actinolite or tremolite), talc, chlorite, dolomite and magnetite; they show pronounced compositional layering on a 10 cm to 10 m scale, possibly reflecting primary igneous layering (Tarney, 1978), in which actinolite-rich rocks (presumably meta-pyroxenites) alternate with talc + chlorite-rich rocks (presumably meta-peridotites).

Background geology

The Achmelvich ultramafic/mafic complex lies within the central 'Scourian' zone of the Lewisian outcrop (Sutton and Watson, 1951), an area which records an extended Archaean and Proterozoic history of intrusion, deformation and metamorphism (Evans and Tarney, 1964; Evans, 1965; Sheraton *et al.*, 1973; Evans and Lambert, 1974; Park and Tarney, 1987; Sills and Rollinson, 1987). The mafic and ultramafic protoliths of the complex were intruded at an early stage (Tarney, 1978) in a major crust-forming episode at *c.* 2900

Ma (Hamilton *et al.*, 1979) and subsequently underwent granulite-facies metamorphism during the 'Badcallian' event, dated at *c.* 2700 Ma (Pidgeon and Bowes, 1968; Moorbath *et al.*, 1975; Chapman and Moorbath, 1977; Humphries and Cliff, 1982). Relict granulite-facies assemblages are preserved locally in the mafic gneisses of the complex (Tarney, 1978), but are rare. The complex records a pervasive amphibolite-facies overprint, the 'Inverian' event of Evans (1965) and Evans and Lambert (1974), which took place during an extended period of slow cooling prior to the intrusion of dolerite dykes (the 'Scourie dykes' of Sutton and Watson, 1959) at *c.* 2400 Ma (Chapman, 1979). The TCPs described in this paper are probably of Inverian age.

Metamorphic conditions during the Inverian event are poorly constrained. On the basis of amphibolite-facies assemblages in muscovite-rich metasediments, Cartwright and Barnicoat (1986) estimate conditions of 3–6 kbar and 625–500°C for the Inverian event in the Achmelvich area. Ultramafic rocks further north in the Scourian zone preserve early Inverian anthophyllite overprinted by later Inverian tremolite + chlorite assemblages, for which Sills (1982) has estimated temperatures of 800–650°C and 650–550°C, respectively. Late amphibolite-facies assemblages in mafic gneisses probably crystallized at temperatures in the range 700–600°C (Sills, 1983).

Mineralogy and petrography

TCPs have been found at three localities in the Achmelvich ultramafic/mafic complex (the grid references of which may be obtained by writing to the author):

Locality 1: The rocks at this small (1.5 m wide) exposure have a distinct layering which dips *c.* 70° to the SE. The TCP-rich rocks mainly occupy the

TABLE 1. Mineral assemblages in selected samples of ultramafic rock from Achmelvich.

Sample No.	In Pyribole Prisms							Matrix Minerals					
	Clinojimthompsonite	Jimthompsonite	Chesterite Polytypes	Tremolite / Actinolite	Hornblende	Cummingtonite	Anthophyllite	Talc	Chlorite	Dolomite	Calcite	Phlogopite	Magnetite
Ach 1A	*		+	*		*	+		*	*			+
Ach 1B	*			*		*	+		*	*			+
Ach 1C	*		?	*		*	+		*	*			*
Ach 1D	*			*		*	+		*	*			+
Ach 1E	?			*	+	*							+
Ach 1F	?			*	+	+			*				+
Ach 2A				*				*	*	*			*
Ach 3				*				*	*	*			*
Ach 4	+			*	+	*	+		*			+	*
Ach 5A				*				*	*	*			*
Ach 5B				*				*	*	*			*
Ach 6B	+	*	*			+	*	R	*		*		+
Ach 7B				*				*	*	*			*
Ach 8A	*		?	*		*	+	R	*	+			+
Ach 8B	*	+		*		*	*	R	*	*			+
Ach 9A	*	+		*		*	+	*	*	*			+
Ach 9B	+			*	+	*		R	*	+			*
Ach 9C	+			*		*		R	*				*
Ach 9F	+	+	?	*		*	+	*	*				*

*: major mineral; +: minor mineral; ?: presence suspected but not confirmed; R; retrogressive alteration product. Where two or more pyribole phases occur in the same rock, they are generally intergrown with one another in compound prisms.

central part of the exposure; they are medium- to coarse-grained unfoliated talc-rich rocks within which the TCPs form randomly oriented, pale brown, acicular to prismatic porphyroblasts up to 3 cm long, mostly with dark green actinolite cores. The sequence of layers is as follows:

South

15 cm Medium-grained grey-green actinolite-granofels (Sample Ach 9B).
8 cm Coarse-grained TCP-chlorite-actinolite-granofels (Ach 9C).
15 cm Medium-grained grey-green actinolite-granofels (Ach 9D).
15 cm Coarse-grained TCP-chlorite-talc-granofels. 2–3 cm long pyribole prisms with actinolite cores (Ach 9A).
40 cm Medium- to coarse-grained knotty TCP-chlorite-talc granofels.
20 cm Medium-grained TCP-chlorite-talc-granofels. Very talc-rich. TCP prisms up to 1 cm long (Ach 9F).
20+ cm Coarse-grained chlorite-actinolite-granofels (Ach 9G).

North

Mineral assemblages of samples Ach 9A, Ach 9B, Ach 9C and Ach 9F are listed in Table 1.

The TCP is best displayed by sample Ach 9A, which will serve as a type. In thin-section, this rock is seen to consist of euhedral compound TCP + amphibole prisms set in a matrix composed dominantly of random, interlocking, sub-equant flakes of magnesian chlorite and talc, with subordinate anhedral dolomite and subhedral magnetite. The majority of the compound prisms have pale green subhedral cores of actinolite and colourless, zoned, coherent overgrowths of TCP ± amphibole (Figs. 1*a,b*) the *b* and *c* axes of which are parallel to the *b* and *c* axes, respectively, of the actinolite. Two main types of overgrowth occur: (1) euhedral wedge-shaped TCP 'wings', measuring up to 1 mm wide in the *b* direction, extending from the {010} faces of the actinolite cores, and (2) somewhat thinner colourless amphibole + TCP overgrowths on the actinolite {110} faces.

The TCP that forms the dominant phase in the 'wings' superficially resembles colourless amphibole except that its cleavage angle in sections highly inclined to the *c* axis is $< 40°$ (Fig. 1*b*), and it locally contains thin (< 10 μm) lamellae parallel to (010). In both these respects, this mineral resembles the type material from Chester (Veblen and Burnham, 1978*a*). It has relatively high birefringence, and generally shows inclined extinction in long section; this phase is identified as clinojimthompsonite (see below). The clinojimthompsonite prism faces are parallel to the cleavage planes (Fig. 1*b*), indicating that the overgrowths are not pseudomorphous after amphibole.

The amphibole-rich overgrowths on the actinolite {110} faces have lower birefringence and a much higher density of (010) lamellae. The host phase is cummingtonite and the (010) lamellae, which range in width from *c.* 10 μm to 0.5 μm and smaller, are probably clinojimthompsonite. Close to their mutual interface, the actinolite and cummingtonite commonly contain lamellae of one another. One set of these lamellae is oriented || (100) (Fig. 1*a*); another set, which is generally only visible in long or oblique sections, resembles the ($\bar{1}01$) lamellae described by Ross *et al.* (1969).

Some of the smaller basal sections appear to lack actinolite cores but retain the characteristic 'wings' of clinojimthompsonite and central cummingtonite 'belts' rich in (010) TCP lamellae, juxtaposed along sharp (010) planes (Fig. 1*g*). In other small basal sections, 'wings' and lamellae of clinojimthompsonite and cummingtonite are distributed asymmetrically. A third type, ususally with {010} prism faces, consists mainly of cummingtonite with subordinate TCP lamellae. Optically continuous clusters of small basal sections are common and may represent sections through acicular terminations of larger compound prisms.

In some large compound prisms, domains of anthophyllite occur in the obtuse angles made by intersecting {110} faces and are separated from the cummingtonite-rich domains by sharp planes parallel to (100) (Fig. 1*a,b*). Where the anthophyllite domain is wide enough to extend as far as the 'wings', it either continues outboard of the clinojimthompsonite or terminates against a wedge-shaped zone of jimthompsonite (Fig. 1*a*). The interface between these two TCP phases is parallel to (100).

Pyribole prisms in sample Ach 9F closely resemble those of Ach 9A except that the orthorhombic amphibole and TCP polytypes appear to be more abundant. In the actinolite-rich granofelses from this locality (Ach 9B and Ach 9C) and from 10 m to the ENE (Ach 4), cummingtonite, locally with thin (010) lamellae, forms irregular rims on actinolite and is intergrown with it on (100) and ?($\bar{1}01$). Discrete clinojimthompsonite 'wings' are rare.

Locality 2: Here, TCP-rich schists form a layer *c.* 45 cm thick at the top of an ultramafic unit, within 1 m of the contact with overlying mafic gneisses. Modal and grain-size layering occur

within the TCP-bearing horizon (see Table 1 for assemblages). The coarsest rocks (samples Ach 1A, Ach 1B and Ach 1C) contain abundant randomly oriented pale brown TCP prisms up to 2 cm long set in schistose matrix. In thin-section, the matrix is seen to consist of fine-grained granoblastic polygonal dolomite grains and aligned flakes of chlorite, commonly concentrated in near-monomineralic layers. The compound pyribole prisms cut across the chlorite schistosity and are evidently post-tectonic. The prisms closely resemble those of Ach 9A except that the actinolite cores are smaller and more obviously intergrown with cummingtonite, and the cummingtonite-rich 'belts' are commonly flanked by multiple 'wings' of clinojimthompsonite (Fig. 1*f*). A few of the small basal sections in Ach 1A show (010) intergrowths of three different phases (as distinguished by birefringence): cummingtonite, clinojimthompsonite, and a phase with birefringence intermediate between the two, probably the monoclinic polytype of chesterite (Fig. 1*e*).

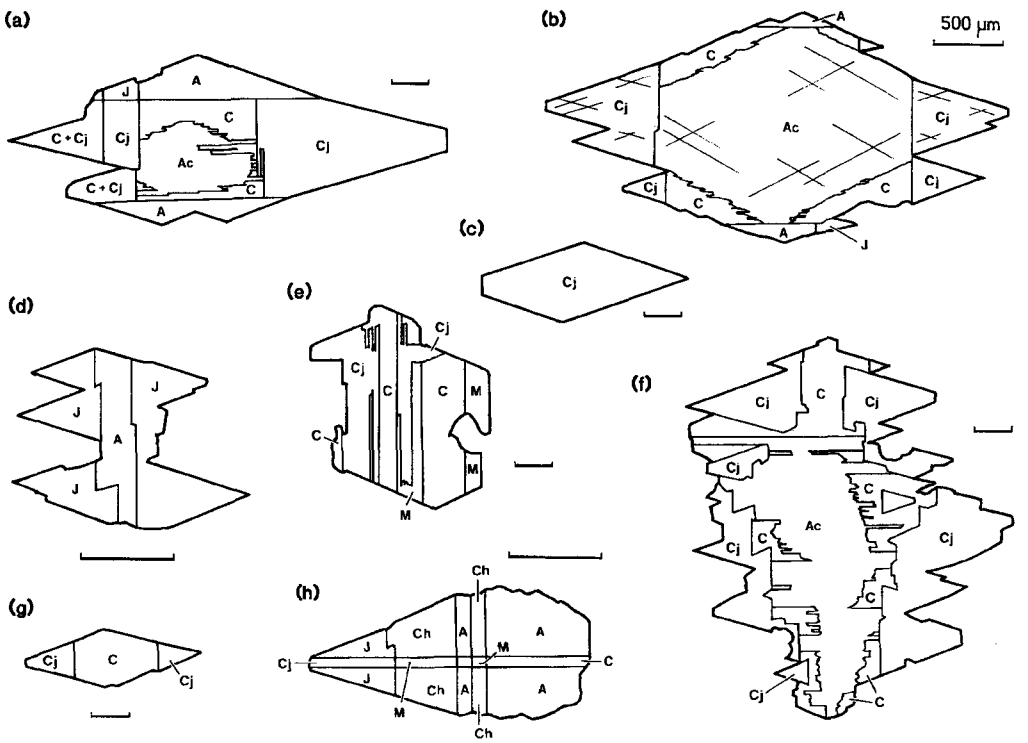

FIG. 1. Varieties of compound pyribole prisms containing parallel intergrowths of triple-chain pyriboles, as observed in rocks at Achmelvich. Partly schematic camera-ready drawings of sections at high angles to the *c*-axis. All scale bars 100 μm unless otherwise stated. Only the dominant phase in each sector of the prism is indicated; subordinate lamellae of other phases have been omitted for clarity. Abbreviations: A, anthophyllite; Ac, actinolite; C, cummingtonite; Ch, chesterite; Cj, clinojimthompsonite; J, jimthompsonite; M, intermediate phase (probably the monoclinic polytype of chesterite. (*a*) Intergrowth of five pyribole phases, including orthorhombic and monoclinic polytypes of both Mg,Fe-amphibole and TCP. Note the obtuse re-entrant angle between the prism faces of the euhedral Cj and A overgrowths. Ach9A. (*b*) Typical prism with large Ac core and Cj 'wings'. Note that the cleavage angle is smaller in the 'wings' than in the core and that cleavage is parallel to the Cj crystal faces. Ach9A. (*c*) One of a cluster of small, optically continuous Cj euhedra. Ach1C. (*d*) Small prism of intergrown orthorhombic phases. Note the central 'belt' of A separated from 'wings' of J by (010) planes. Ach6B. (*e*) Three monoclinic low-Ca pyriboles intergrown along (010). Ach1C. (*f*) Complex prism with multiple Cj 'wings' on an irregular central 'belt' in which Ac and C are extensively intergrown on (100). Ach1C. (*g*) Small euhedral prism with 'belt' of C and 'wings' of Cj. Ach9A. (*h*) Intergrowth of six low-Ca pyriboles. Note that pyriboles of different chain-width type are separated by (010) planes, while orthorhombic and monoclinic polytypes of each chain-width type are separated by (100) planes. Ach6B.

Other samples (Ach 8A and Ach 8B), from a different part of the same TCP-bearing horizon, are not schistose but otherwise resemble those described above.

Locality 3: This locality is a 0.5 m wide exposure of medium-grained TCP-rich rock adjacent to a prominent mafic gneiss horizon. Compound TCP + amphibole prisms form a mesh of pale 1 cm long needles set in a grey calcite-rich matrix. In thin-section (sample Ach 6B), the prisms are seen to consist predominantly of orthorhombic pyriboles (Fig. 1*d*), with monoclinic varieties confined to thin median (100) lamellar domains (Fig. 1*h*). Actinolite is believed to be absent. Both orthorhombic and monoclinic domains are composed of (010) lamellae, with up to three different phases (distinguished by birefringence) visible in each (Fig. 1*h*). As at the previous two localities, pyribole basal sections commonly show 'wings' of high-birefringence TCP with cleavage angles < 40°, here mainly of jimthompsonite with subordinate clinojimthompsonite. The (010) lamellae with the lowest birefringence in basal sections are of anthophyllite with minor cummingtonite. The (010) lamellae with intermediate birefringence probably consist of chesterite and its monoclinic polytype.

Identification of triple-chain pyriboles

The identification of the TCP phases is based primarily on cleavage angle, X-ray diffraction data, back-scattered electron intensity, and extinction angle. Chemical analyses (see below), though not diagnostic on their own, support the identifications.

Cleavage angles

Veblen and Burnham (1978*a*) pointed out that cleavage angles could be used to distinguish jimthompsonite polytypes from those of chesterite and from amphiboles. They measured acute cleavage angles of 37.8° and 44.7° for jimthompsonite {210} and chesterite {110} respectively.

The angle between the two cleavages in TCP basal sections (i.e. perpendicular to the *c*-axis) in the Achmelvich samples was measured by (a) using the revolving stage on the petrographic microscope, and (b) protractor measurements on back-scattered electron micrographs. In sample Ach 9A, basal sections of compound actinolite + cummingtonite + TCP prisms that showed acute cleavage angles of 56 ±1° in the actinolite cores gave acute angles of 38 ± 1° in the TCP 'wings'. The average of 15 measurements was 38.2°. Similar relationships were observed in samples Ach 1A, Ach 1B, Ach 1C, Ach 1D, Ach 6B, Ach 8A, Ach 8B, Ach 9C and Ach 9F. The cleavage angle obtained here is very close to the jimthompsonite value, indicating the presence, in each case, of at least one of the jimthompsonite polytypes.

Cleavage angles could not be measured in the chesterite-like lamellae in Ach 6B and Ach 1A.

X-ray data

Scanning diffractograms of powdered hand-picked TCP overgrowths from Ach 9A showed peaks (in order of decreasing intensity) at 3.08, 8.80, 3.24, 4.53, 4.39, 13.6, 2.93, 2.97, 2.61, 2.23, 2.63, and 6.80 Å, which match well, respectively, with calculated (310), (110), ($\bar{2}$60), (060), (220), (020), (330), ($\bar{3}$31), ($\bar{1}$91), ($\bar{1}$*11*) ($\bar{1}$12) and (040) peak positions of clinojimthompsonite (Veblen and Burnham, 1978*a*) as listed in the ASTMS data file. All peaks except those at 2.97 and 2.63 Å can also be indexed for jimthompsonite, but the match is less good. The following lattice parameters were calculated from these data using the least squares program CELL (T.J.B. Holland, unpubl.), assuming monoclinic symmetry: a = 9.862 ± 0.008 (2σ), b = 27.184 ± 0.020, c = 5.298 ± 0.004 Å, β = 109.61° ± 0.14°, cell volume = 1337.9 ± 1.8 Å^3. The TCP overgrowths from Ach 1C gave identical results within the errors quoted. The c parameter and cell volume are significantly smaller than the values given by Veblen and Burnham (1978*a*) (5.32 Å and 1347 Å^3, respectively), which is probably a reflection of the fact that the Achmelvich clinojimthompsonite has a higher Mg/Fe ratio than that from Chester (see below).

The presence of jimthompsonite, chesterite and the monoclinic polytype of chesterite could not be confirmed by X-ray work.

Extinction angle

In all TCP-bearing samples except Ach 6B (Table 1), the dominant TCP phase showed inclined extinction in sections at high angles to the b axis. The measured value of the angle γ:c is 10°, which is identical to the figure given by Veblen and Burnham (1978*a*) for clinojimthompsonite, and is significantly lower than the typical values for the Mg-rich clino-amphiboles tremolite (15–21°) and cummingtonite (16–20°) (Deer *et al.*, 1992).

The dominant TCP phase in the 'wings' of Ach 6B pyribole prisms has straight extinction in sections parallel to c, but otherwise bears close optical resemblance to clinojimthompsonite. In view of cleavage angle considerations (see above),

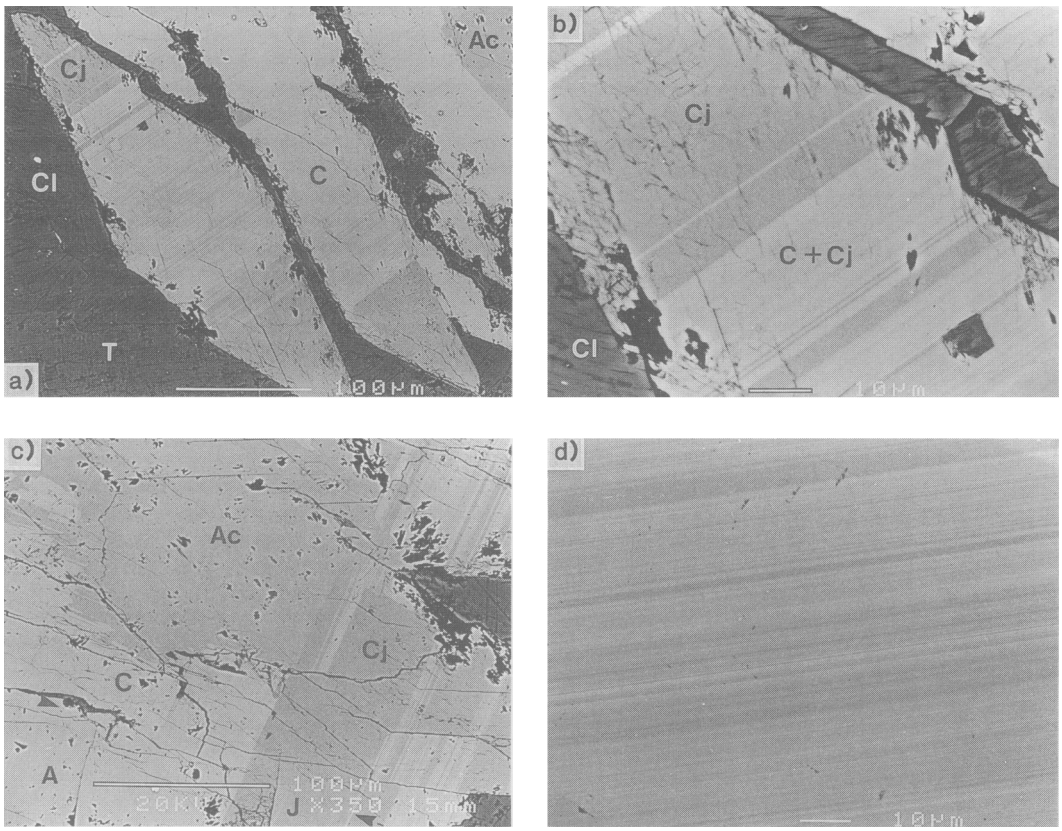

FIG. 2. Back-scattered electron-micrographs of intergrown pyriboles in Ach9A. (*a*) Basal sections of small prisms containing cummingtonite (C), appearing pale, and clinojimthompsonite (Cj), appearing grey, intergrown on (010). Note the large number of (010) lamellae in the central C-rich 'belt' compared with the Cj 'wings'. Part of a core of actinolite (Ac) is visible in one prism. The matrix consists of chlorite (Cl), talc (T) and magnetite (white). (*b*) High-power view of part of 2*a* showing the interface between the clinojimthompsonite 'wing' regions with few (010) lamellae and the cummingtonite-rich 'belt' (C + Cj) in which the two phases are intergrown on (010) on scales of 1 μm and smaller. Cl: chlorite. Scale bar 10 μm. (*c*) Central part of the prism shown in Fig. 1*a*. Section almost perpendicular to *c* axis. Note that the cleavage angle shown by the actinolite (Ac) in the core is larger than that shown by the clinojimthompsonite region (Cj). The actinolite is intergrown with cummingtonite (C) on (010). J, jimthompsonite; A, anthophyllite. The (100) boundary that separates the orthorhombic and monoclinic domains lies along the line of the arrows. Scale bar 100 μm. Scale factor incorrect. (*d*) High-power view of laterally continuous μm-scale (010) lamellae, probably of cummingtonite (light) and clinojimthompsonite (dark), in the centre of a small prism.

this phase is identified as jimthompsonite. In Ach 9A, jimthompsonite can be distinguished from the more abundant clinojimthompsonite by the fact that, in oblique basal sections, it extinguishes in the same position as anthophyllite, with which it is invariably in contact.

BSE intensity

The intensity of back-scattered electron (BSE) radiation is mainly a function of average atomic number ($\bar{Z}$) and, to a lesser extent, lattice orientation (Lloyd, 1987). In parallel intergrowths of pyribole phases, such as occur in the samples described here, orientation contrast is minimal, and contrast is determined almost entirely by differences in $\bar{Z}$. In Mg-rich biopyriboles, $\bar{Z}$-contrast is controlled mainly by hydrogen content and Fe/Mg ratio.

BSE micrographs of biopyriboles in samples Ach 9A (Fig. 2), Ach 1A and Ach 6B (Fig. 3) were obtained on a Jeol JSM 6400 scanning electron

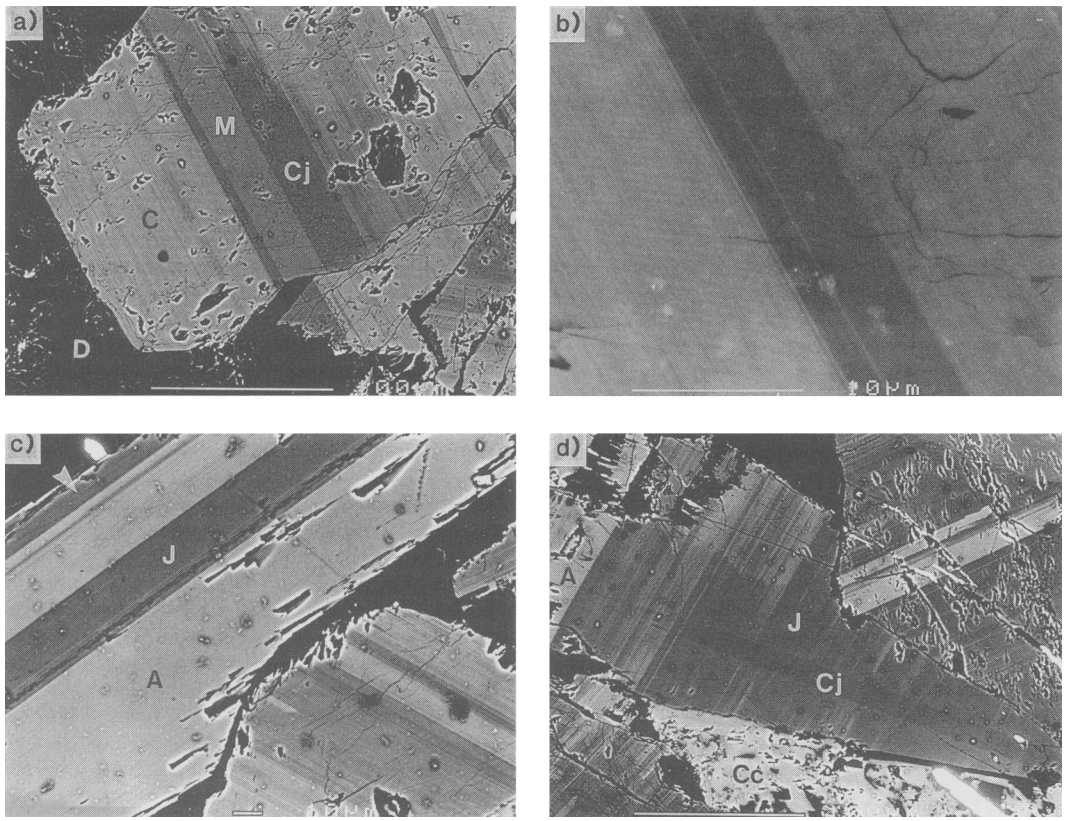

FIG. 3. Back-scattered electron-micrographs of intergrown pyriboles (cont'd.) (*a*) Basal section of a prism containing three monoclinic pyriboles intergrown on (010): cummingtonite (C), clinojimthompsonite (Cj) and an intermediate phase (M), probably the monoclinic polytype of chesterite. D, dolomite. Scale bar 100 μm. Ach1A. (*b*) High-magnification view of part of Fig. 3*a* showing (010) lamellae with thicknesses of c. 0.1 μm in all three domains. (*c*) Anthophyllite (A) and jimthompsonite (J) in a section cut at a high angle to the *a*-axis. The lamella with intermediate contrast (arrowed) is probably chesterite. Ach6B. (*d*) Oblique section through the 'wing' region of a prism, showing a median (100) lamella of clinojimthompsonite (Cj) within slightly paler (higher $\bar{Z}$) jimthompsonite (J). Cc, calcite; A, anthophyllite. Scale bar 100 μm. Ach6B.

microscope operating at 20 kV with a working distance of 15 mm.

The presence of pyriboles chemically intermediate between talc and anthophyllite is confirmed by BSEM. The TCP phases in BSE micrographs of Ach 9A are much brighter than talc and chlorite, but darker than Mg,Fe-amphiboles (Fig. 2*a,b,c*). Optically identified jimthompsonite and clinojimthompsonite are generally indistinguishable in BSE images, as are anthophyllite and cummingtonite; under high-contrast conditions, however, the orthorhombic polytypes appear slightly brighter than their monoclinic equivalents (e.g. Fig. 3*d*). In the small compound prisms containing three phases intergrown on (010) in Ach 1A and Ach 6B, the lamellae that have birefringence intermediate between those of Mg,Fe-amphibole and jimthompsonite polytypes also show intemediate BSE intensity (Fig. 3*a,b,d*), consistent with the existence of one or both chesterite polytypes.

Optical properties of clinojimthompsonite

Due to the small volumes of clinojimthompsonite in the Chester pyriboles, Veblen and Burnham (1978*a*) were unable to determine fully the optical properties of this mineral.

Refractive indices of clinojimthompsonite were estimated by immersing oriented crystal fragments

TABLE 2. Microprobe analyses of pyriboles and associated silicate minerals in sample Ach9A. All Fe assumed to be Fe^{++}. M = Mg/(Mg+Fe+Mn). $\bar{Z}$ = mean atomic number, calculated using equation 4 of Lloyd (1987).

	Clinojimthompsonite						Jimthompsonite		
	1	2	3	4	5	6	1	2	3
SiO_2	58.57	58.27	58.67	58.12	58.86	58.82	58.86	58.57	58.64
TiO_2	0.03	0.00	0.00	0.08	0.05	0.08	0.09	0.00	0.00
Al_2O_3	0.30	0.35	0.34	0.32	0.41	0.28	0.22	0.12	0.27
Cr_2O_3	0.00	0.07	0.00	0.00	0.01	0.16	0.01	0.14	0.00
FeO	10.88	10.86	10.43	10.50	10.77	10.23	10.52	10.65	10.31
MnO	0.41	0.37	0.39	0.47	0.56	0.37	0.39	0.42	0.41
MgO	25.74	25.68	25.78	25.52	25.81	25.63	26.38	26.21	26.09
CaO	0.50	0.53	0.51	0.43	0.55	0.39	0.24	0.31	0.19
Na_2O	-	-	-	-	-	0.24	-	-	0.07
K_2O	0.00	0.00	0.00	0.07	0.08	0.07	0.00	0.00	0.03
Total	96.43	96.13	96.12	95.51	97.10	96.27	96.71	96.14	96.01
Formula	34(O)	34(O)	34(O)	34(O)	34(O)	34(O)	34(O)	34(O)	34(O)
Si	11.99	11.97	12.02	12.00	11.97	12.03	11.99	11.98	12.02
Ti	0.01	0.00	0.00	0.01	0.01	0.01	0.01	0.00	0.00
Al	0.07	0.09	0.08	0.08	0.10	0.07	0.05	0.03	0.07
Cr	0.00	0.01	0.00	0.00	0.00	0.03	0.00	0.02	0.00
Fe	1.86	1.87	1.79	1.81	1.83	1.75	1.79	1.82	1.77
Mn	0.07	0.06	0.07	0.08	0.10	0.06	0.07	0.07	0.07
Mg	7.85	7.87	7.87	7.86	7.83	7.82	8.01	7.99	7.97
Ca	0.11	0.12	0.11	0.09	0.12	0.08	0.05	0.07	0.04
Na	-	-	-	-	-	0.10	-	-	0.01
K	0.00	0.00	0.00	0.02	0.02	0.02	0.00	0.00	0.01
Total	21.96	21.99	21.94	21.95	21.98	21.97	21.97	21.98	21.98
M	0.80	0.80	0.81	0.81	0.80	0.81	0.81	0.81	0.80
$\bar{Z}$	11.89	11.90	11.85	11.87	11.90	11.83	11.83	11.86	11.82

	Cummingtonite		Anthophyllite		Actinolite		Talc		Chlorite
	1	2	1	2	1	2	1	2	1
SiO_2	57.25	57.79	57.14	56.63	55.61	53.63	62.60	62.44	29.11
TiO_2	0.00	0.09	0.07	0.00	0.08	0.09	0.00	0.05	0.02
Al_2O_3	0.15	0.13	0.18	0.25	2.09	3.85	0.24	0.18	19.39
Cr_2O_3	0.03	0.00	0.00	0.02	0.27	0.24	0.00	0.00	0.39
FeO	14.45	14.24	13.60	12.44	5.20	6.67	2.90	2.88	7.23
MnO	0.53	0.59	0.64	0.39	0.24	0.19	0.00	0.00	0.05
MgO	24.98	24.75	25.34	25.56	20.79	19.24	29.33	29.16	29.12
CaO	0.56	0.68	0.29	0.40	12.33	11.75	0.00	0.00	0.01
Na_2O	-	-	-	0.24	0.51	0.76	-	-	-
K_2O	0.00	0.03	0.00	0.00	0.05	0.01	0.01	0.00	0.00
Total	97.95	98.30	97.26	95.93	97.17	96.43	95.08	94.71	85.32
Formula	23(O)	23(O)	23(O)	23(O)	23(O)	23(O)	11(O)	11(O)	14(O)
Si	7.97	8.01	7.98	7.98	7.77	7.60	4.01	4.01	2.86
Ti	0.00	0.01	0.01	0.00	0.01	0.01	0.00	0.00	0.00
Al	0.02	0.02	0.03	0.04	0.35	0.64	0.02	0.01	2.25
Cr	0.00	0.00	0.00	0.00	0.03	0.03	0.00	0.00	0.03
Fe	1.68	1.65	1.59	1.47	0.61	0.79	0.16	0.16	0.59
Mn	0.06	0.07	0.08	0.05	0.03	0.02	0.00	0.00	0.00
Mg	5.19	5.11	5.28	5.37	4.33	4.07	2.80	2.79	4.27
Ca	0.08	0.10	0.04	0.06	1.85	1.79	0.00	0.00	0.00
Na	-	-	-	0.07	0.14	0.21	-	-	-
K	0.00	0.01	0.00	0.00	0.01	0.00	0.00	0.00	0.00
Total	15.00	14.98	15.01	15.04	15.13	15.16	6.99	6.97	10.00
M	0.75	0.75	0.76	0.78	0.87	0.83	0.95	0.95	0.88
$\bar{Z}$	12.33	12.33	12.25	12.11	12.00	12.13	10.86	10.85	11.06

TABLE 3. Microprobe analyses of pyriboles and associated silicate minerals in sample Ach1A. The intermediate phase is probably the monoclinic polytype of chesterite. Cumm: cummingtonite. Anth: anthophyllite. Actin: actinolite. All Fe assumed to be Fe^{++}. M = Mg/(Mg+Fe+Mn). $\bar{Z}$ = mean atomic number, calculated using equation 4 of Lloyd (1987).

	Clinojimthompsonite			Intermediate Ph.		Cumm.	Anth.	Actin.	Chlorite
	1	2	3	1	2	1	1	1	1
SiO_2	58.46	58.42	59.18	58.15	58.68	57.90	57.79	54.21	29.27
TiO_2	0.04	0.00	0.09	0.00	0.02	0.12	0.00	0.10	0.04
Al_2O_3	0.00	0.00	0.00	0.00	0.00	0.15	0.00	3.60	20.34
Cr_2O_3	0.10	0.12	0.22	0.00	0.16	0.05	0.17	0.50	1.18
FeO	11.89	12.25	11.64	13.18	13.70	14.66	14.39	6.20	9.07
MnO	0.46	0.32	0.45	0.31	0.19	0.43	0.36	0.08	0.11
MgO	25.14	24.92	25.51	25.00	24.94	24.39	24.98	19.61	27.90
CaO	0.62	0.54	0.25	0.31	0.26	0.51	0.46	12.00	0.09
Na_2O	0.00	0.00	0.00	0.52	0.27	0.14	0.00	0.99	0.00
K_2O	0.03	0.06	0.00	0.00	0.00	0.00	0.04	0.00	0.03
Total	96.74	96.63	97.34	97.47	98.22	98.35	98.19	97.29	88.03
Formula	34(O)	34(O)	34(O)	57(O)	57(O)	23(O)	23(O)	23(O)	14(O)
Si	12.01	12.02	12.04	20.01	20.04	8.03	8.01	7.61	2.82
Ti	0.01	0.00	0.01	0.00	0.01	0.01	0.00	0.01	0.00
Al	0.00	0.00	0.00	0.00	0.00	0.02	0.00	0.60	2.31
Cr	0.02	0.02	0.04	0.00	0.04	0.01	0.02	0.06	0.09
Fe	2.04	2.11	1.98	3.79	3.91	1.70	1.67	0.73	0.73
Mn	0.08	0.06	0.08	0.09	0.05	0.05	0.04	0.01	0.01
Mg	7.70	7.64	7.73	12.82	12.70	5.04	5.16	4.10	4.01
Ca	0.14	0.12	0.05	0.11	0.10	0.08	0.07	1.81	0.01
Na	0.00	0.00	0.00	0.35	0.18	0.04	0.00	0.27	0.00
K	0.01	0.02	0.00	0.00	0.00	0.00	0.01	0.00	0.00
Total	22.01	21.99	21.93	37.17	37.03	14.98	14.98	15.20	9.98
M	0.78	0.78	0.79	0.77	0.76	0.74	0.75	0.85	0.84
$\bar{Z}$	12.04	12.06	11.98	12.13	12.18	12.35	12.32	12.10	11.34

in R.I. oils, viewing them in sodium light, and applying the Becke line method. The lateral overgrowths from sample Ach 9A gave α: 1.600, β: 1.619 and γ: 1.628, while crystals from Ach 1A gave α: 1.604, β: 1.622 and γ: 1.632 (all measurements $\pm$ 0.001). The maximum birefringence (γ–α) was checked by using a Berek compensator to measure the retardation of appropriate crystals in polished sections of known thickness (measured by micrometer gauge); clinojimthompsonite from Ach 1A, Ach 1B and Ach 1C all yielded maximum birefringence values of 0.027, consistent with the refractive index data.

The optical orientation of clinojimthompsonite is $\beta \parallel b$, (i.e. optic axial plane $\parallel$ (010)), and the optic sign is negative. The optic axial angle, $2V_\alpha$, was measured by U-stage; the 'wing' regions in a crystal from sample Ach 1A gave a value of 67 $\pm$ 2°, which is consistent with the measured refractive indices, within error.

Clinojimthompsonite is colourless in thin-section but thick crystal fragments show weak pleochroism with α (colourless) < β (very pale brown) < γ (pale pinkish brown).

Mineral chemistry

Major-element compositions of pyriboles and coexisting minerals in samples Ach 9A, Ach 1A and Ach 6B were determined by electron microprobe. Coexisting tremolite, chlorite, talc and dolomite in TCP-free sample Ach 5A were also analysed.

Analyses (Tables 2, 3, 4 and 5) were performed on a Cameca Camebax electron microprobe fitted with Link AN10000 software, operating at 15 kV. For all samples except Ach 6B, Mg, Fe, Al and Si were determined by wavelength-dispersive spectrometry using periclase, fayalite, corundum and wollastonite standards, respectively; all other elements were analysed by energy-dispersive

TABLE 4. Microprobe analyses of pyriboles in sample Ach6B. All Fe assumed to be Fe^{++}. M = Mg/(Mg+Fe+Mn). $\bar{Z}$ = mean atomic number, calculated using equation 4 of Lloyd (1987).

	Jimthompsonite			? Chesterite			Anthophyllite		
	1	2	3	1	2	3	1	2	3
SiO_2	59.15	59.12	58.36	58.90	58.64	58.82	57.71	58.00	57.34
TiO_2	0.00	0.00	0.03	0.10	0.00	0.00	0.00	0.15	0.00
Al_2O_3	0.00	0.03	0.00	0.39	0.00	0.07	0.00	0.00	0.00
Cr_2O_3	0.09	0.07	0.00	0.09	0.10	0.00	0.00	0.00	0.07
FeO	10.86	10.68	10.88	11.89	12.32	12.18	14.36	13.72	13.79
MnO	0.41	0.56	0.30	0.00	0.43	0.25	0.38	0.41	0.31
MgO	26.08	26.12	25.86	25.98	25.86	26.29	25.25	25.23	26.04
CaO	0.42	0.56	0.60	0.40	0.22	0.39	0.34	0.51	0.34
Total	97.01	97.14	96.03	97.75	97.57	98.00	98.04	98.02	97.89
Formula	34(O)	34(O)	34(O)	57(O)	57(O)	57(O)	23(O)	23(O)	23(O)
Si	12.03	12.01	12.00	20.00	20.03	19.99	8.01	8.03	7.96
Ti	0.00	0.00	0.01	0.03	0.00	0.00	0.00	0.02	0.00
Al	0.00	0.01	0.00	0.16	0.00	0.03	0.00	0.00	0.00
Cr	0.02	0.01	0.00	0.02	0.03	0.00	0.00	0.00	0.01
Fe	1.85	1.82	1.87	3.38	3.52	3.46	1.67	1.59	1.60
Mn	0.07	0.10	0.05	0.00	0.12	0.07	0.05	0.05	0.04
Mg	7.91	7.91	7.93	13.15	13.17	13.32	5.22	5.20	5.39
Ca	0.09	0.12	0.13	0.15	0.08	0.14	0.05	0.08	0.05
Total	21.97	21.98	21.99	36.89	36.95	37.01	15.00	14.97	15.05
M	0.80	0.80	0.81	0.80	0.78	0.79	0.75	0.76	0.77
$\bar{Z}$	11.89	11.89	11.89	11.97	12.05	12.01	12.30	12.25	12.23

spectrometry (EDS) using a cobalt standard. EDS was used throughout for Ach 6B.

The chemical data of Veblen and Burnham (1978*a*) and Schumacher and Czank (1987) indicate that the bulk of the compositional variation among the wide-chain Mg,Fe-pyriboles may be expressed by the two quantities M = Mg/(Mg+Fe+Mn) and J = [Mg+Fe+Mn+Ca+0.5(Al+Cr)] / Σ cations. The quantity J is simply the ratio of total octahedral cations to total cations, with the assumption that the trivalent ion occupancies are governed by Tschermak substitution, as in Na-free amphiboles. Because J varies with the proportion of M and P layer modules in the biopyribole structure, in principle it should be possible to use this quantity as a means of identification. The J values of ideal stoichiometric Mg,Fe-biopyriboles are as follows: orthopyroxene: 0.5; amphiboles: 0.467; chesterite: 0.459; jimthompsonite: 0.455; talc: 0.429.

Because of the very fine intergrowths commonly present, it has proved difficult to obtain reliable analyses of individual TCP phases, even though analysis spots were routinely chosen from areas apparently devoid of BSE contrast. This, together with the fact that the J values of stoichiometric amphibole, chesterite and jimthompsonite are similar, means that micro-

TABLE 5. Microprobe analyses of minerals in sample Ach 5A. All Fe assumed to be Fe^{++}. M = Mg/(Mg+Fe+Mn).

	Tremolite	Talc	Chlorite	Dolomite
SiO_2	58.18	62.85	31.72	-
TiO_2	0.06	0.00	0.00	-
Al_2O_3	0.30	0.17	16.24	-
Cr_2O_3	0.04	0.00	0.37	-
FeO	2.68	2.14	5.71	2.00
MnO	0.21	0.11	0.00	0.54
MgO	22.82	29.87	31.55	19.23
CaO	13.02	0.03	0.00	31.23
Na_2O	0.00	0.24	-	-
K_2O	0.00	0.00	0.00	-
Total	97.31	95.41	85.59	53.00
Formula	23(O)	11(O)	14(O)	2(O)
Si	7.99	4.00	3.08	-
Ti	0.01	0.00	0.00	-
Al	0.05	0.01	1.86	-
Cr	0.00	0.00	0.03	-
Fe	0.31	0.11	0.46	0.05
Mn	0.02	0.01	0.00	0.01
Mg	4.67	2.84	4.56	0.90
Ca	1.92	0.00	0.00	1.04
Na	0.00	0.03	-	-
K	0.00	0.00	0.00	-
Total	14.97	7.00	9.99	2.00
M	0.93	0.96	0.91	0.93

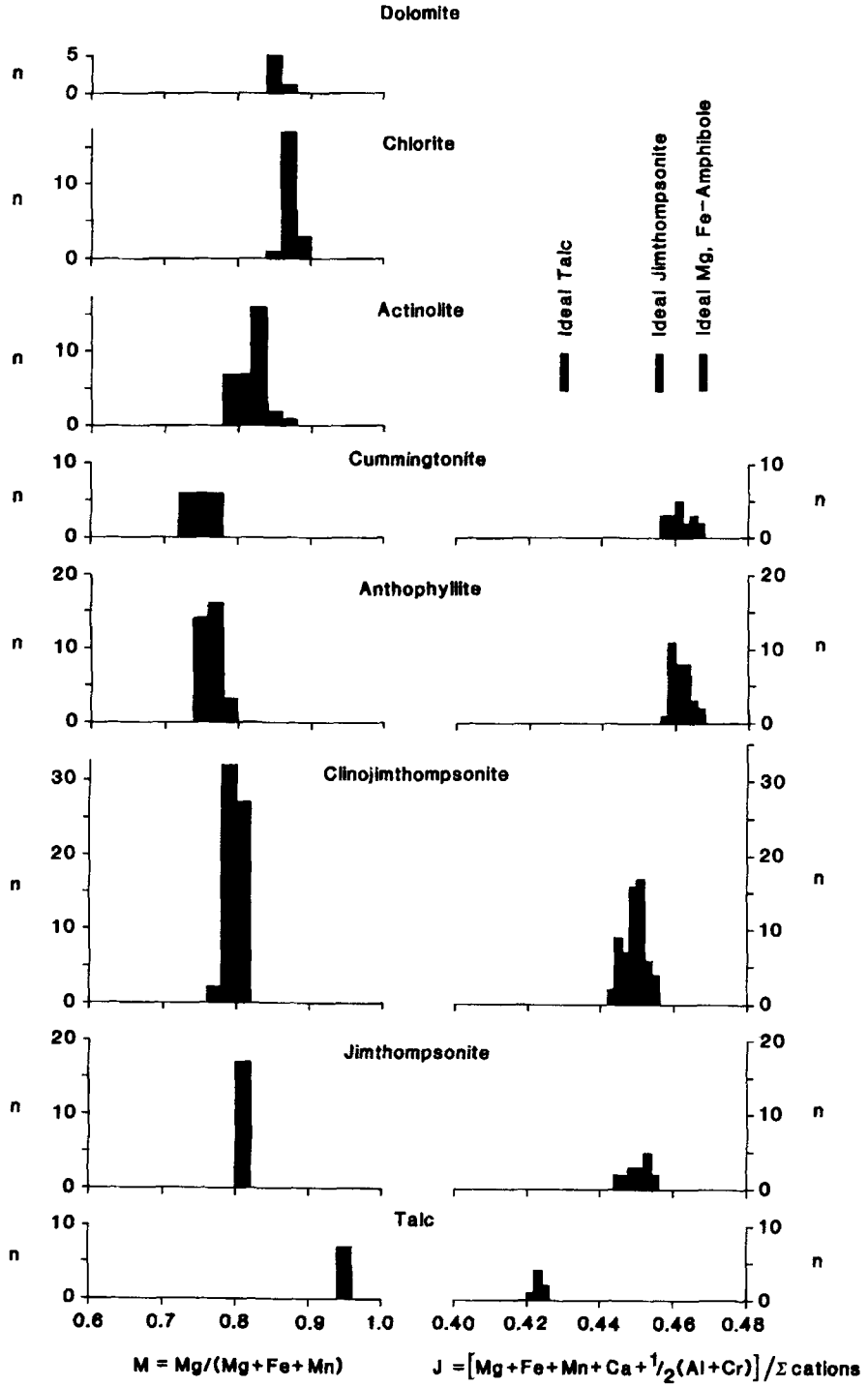
Dolomite
Chlorite
Actinolite
Cummingtonite
Anthophyllite
Clinojimthompsonite
Jimthompsonite
Talc
n
Ideal Talc
Ideal Jimthompsonite
Ideal Mg, Fe-Amphibole
0.6
0.7
0.8
0.9
1.0
0.40
0.42
0.44
0.46
0.48
M = Mg/(Mg+Fe+Mn)
J = [Mg+Fe+Mn+Ca+1/2(Al+Cr)]/Σ cations

probe analysis is of limited use as a primary means of pyribole identification. Analyses with nearly ideal stoichiometry, within analytical error, (such as those listed in Tables 2, 3 and 4) are exceptional. Nevertheless, optically identified populations of Fe,Mg-amphiboles and jimthompsonite polytypes in sample Ach 9A show distinct chemical differences, as reflected by J (Figs. 4,5). The large and significant spread of J values within each population is probably due to local variations in the volume proportion of sub-microscopic lamellae of other phases. Analyses of intermediate phases (tentatively identified as chesterite and its monoclinic polytype) in Ach 1A and Ach 6B give ranges in J value that overlap substantially with those of amphibole and with those of jimthompsonite polytypes, and are therefore non-diagnostic. The TCPs from Achmelvich are slightly more magnesian (i.e. have higher M values) than those from Chester (Veblen and Burnham, 1978a) and less magnesian than those from Orijärvi (Schumacher and Czank, 1987). The M values of respective phases in Ach 9A and Ach 6B are almost identical, and are slightly higher than those in Ach 1A. Within each sample there is a systematic variation in M: talc > chlorite > dolomite > jimthompsonite polytypes > chesterite polytypes > Mg,Fe-amphiboles (Tables 2, 3, 4; Figs. 4, 5). This trend was also noted for pyriboles by Veblen and Burnham (1978*a*) who ascribed it to the combined effect of (a) the tendency of Fe, Mn and Ca to be concentrated in the distorted octahedral sites, and of Mg to be concentrated in the more regular octahedral sites, and (B) the increase in the ratio of regular to distorted octahedral sites with increasing silicate chain-width. The actinolite cores in compound pyribole prisms in Ach 9A and Ach 1A are zoned from relatively Fe-rich centres to more Mg-rich rims, and show large ranges in M-value that overlap with those of chlorite, dolomite and TCPs (Fig. 4).

The $\bar{Z}$ values were calculated from microprobe analyses using equation 4 of Lloyd (1987), assuming stoichiometric hydrogen contents, and are given in tables 2, 3 and 4. Calculated $\bar{Z}$ values for silicates from individual rocks increase in the order talc < chlorite < jimthompsonite polytypes < actinolite < chesterite polytypes < Mg,Fe-amphiboles, and are consistent with observed trends in BSE intensity (Figs. 2, 3).

Small, barely significant chemical differences also exist between orthorhombic and monoclinic polytypes of each pyribole type within a given sample. Orthorhombic polytypes generally have higher M values and lower Ca contents than their monoclinic counterparts (Table 2, Fig. 4) and, consequently, give lower calculated $\bar{Z}$ values (Tables 2, 3). Intriguingly, high-contrast BSE micrographs (e.g. Fig. 3*d*) indicate the reverse. The reason for this inconsistency is not known, but may be due to orientation contrast or systematic differences in unanalysed minor elements.

Physical conditions of pyribole growth

In this section, an attempt is made to estimate the pressure and temperature conditions of metamorphism at the time of pyribole crystallization at Achmelvich, using information from the ultramafic rocks of the complex. As discussed below, the mineral assemblages of the TCP-bearing rocks themselves evidently do not represent equilibrium parageneses and cannot therefore be used for thermobarometry. In the TCP-free samples, the only petrogenetically significant paragenesis is tremolite + talc + chlorite + dolomite (present in Ach 2, Ach 3, Ach 5A, Ach 5B and Ach 7, see Table 1), the stability of which depends on P, T and fluid composition. At all but very low values of X_{CO_2} (assuming that the fluid is a binary H_2O–CO_2 mixture) this paragenesis is limited by the following reactions:

$$\underset{\text{dolomite}}{2\,CaMg(CO_3)_2} + \underset{\text{talc}}{Mg_3Si_4O_{10}(OH)_2} + \underset{\text{quartz}}{4\,SiO_2} = \underset{\text{tremolite}}{Ca_2Mg_5Si_8O_{22}(OH)_2} + \underset{\text{fluid}}{4\,CO_2} \quad (1)$$

$$\underset{\text{dolomite}}{10\,CaMg(CO_3)_2} + \underset{\text{talc}}{13\,Mg_3Si_4O_{10}(OH)_2} = \underset{\text{forsterite}}{12\,Mg_2SiO_4} + \underset{\text{tremolite}}{5\,Ca_2Mg_5Si_8O_{22}(OH)_2} + \underset{\text{fluid}}{20\,CO_2 + 8\,H_2O} \quad (2)$$

$$\underset{\text{chlorite}}{4\,Mg_5Al_2Si_3O_{10}(OH)_8} + \underset{\text{talc}}{11\,Mg_3Si_4O_{10}(OH)_2} = \underset{\text{anthophyllite}}{7\,Mg_7Si_8O_{22}(OH)_2} + \underset{\text{spinel}}{4\,MgAl_2O_4} + \underset{\text{fluid}}{20\,H_2O}. \quad (3)$$

FIG. 4. Mineral compositions in sample Ach9A, plotted as histograms of the two main variables: M = Mg/(Mg + Fe + Mn) and J = [Mg + Fe + Mn + Ca + 0.5(Al+Cr)]/Σ cations, the latter for Mg,Fe-biopyriboles only. Column width = 2σ. Note (i) the large and significant spreads in J value for the amphiboles and the jimthompsonite polytypes, and (ii) the tendency for the orthorhombic pyriboles to have slightly higher M values than their monoclinic polytypes.

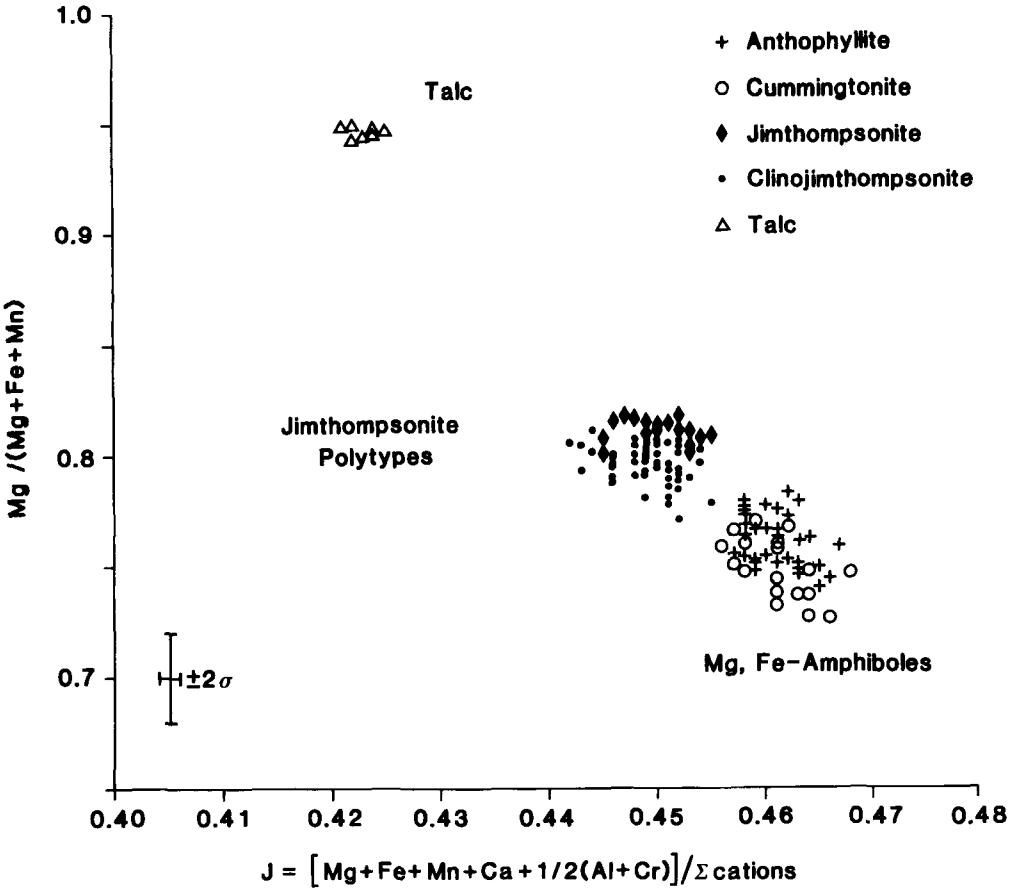

FIG. 5. Graph of M value against J value for Mg,Fe-biopyriboles in sample Ach9A. Error bars are analytical uncertainties ($\pm 2\sigma$) on each point. Note the clear separation of amphibole and TCP fields, despite the large spread in J values in each. Note also the overall inverse correlation between M and J.

Reaction (1) forms the low-T stability limit of the assemblage, reactions (2) and (3) the high-T limit. Figure 6 shows the positions of the equilibrium curves of these reactions calculated using the thermodynamic data of Holland and Powell (1990) for a pressure of 6 kbar and for real mineral compositions in sample Ach 5A. Ideal ionic mixing was assumed for tremolite, talc and chlorite, as formulated by Holland and Powell (1990), and activities of absent phases were set at unity. The assemblage is clearly stable over a wide range of T and X_{CO_2} values at a given P. The maximum T is controlled by the indifferent crossing of curves (2) and (3) and decreases from *c.* 800°C at 8 kbar to *c.* 600°C at 4 kbar (Fig. 6); the minimum T is controlled by the intersection of curves of high dT/dX_{CO_2} at very low X_{CO_2} and is at least 200°C lower than the maximum at any given P. None of the equilibria provides any constraints on pressure.

The results are entirely consistent with those of Cartwright and Barnicoat (1986) for Inverian P–T conditions in the Achmelvich area, and indicate that TCP crystallization was not the result of an 'unusual' set of metamorphic conditions.

Causes of pyribole crystallization

The pyriboles jimthompsonite, chesterite, anthophyllite and their monoclinic polytypes have compositions that lie within the chemical system MgO–FeO–SiO_2–H_2O, as does talc. The existence

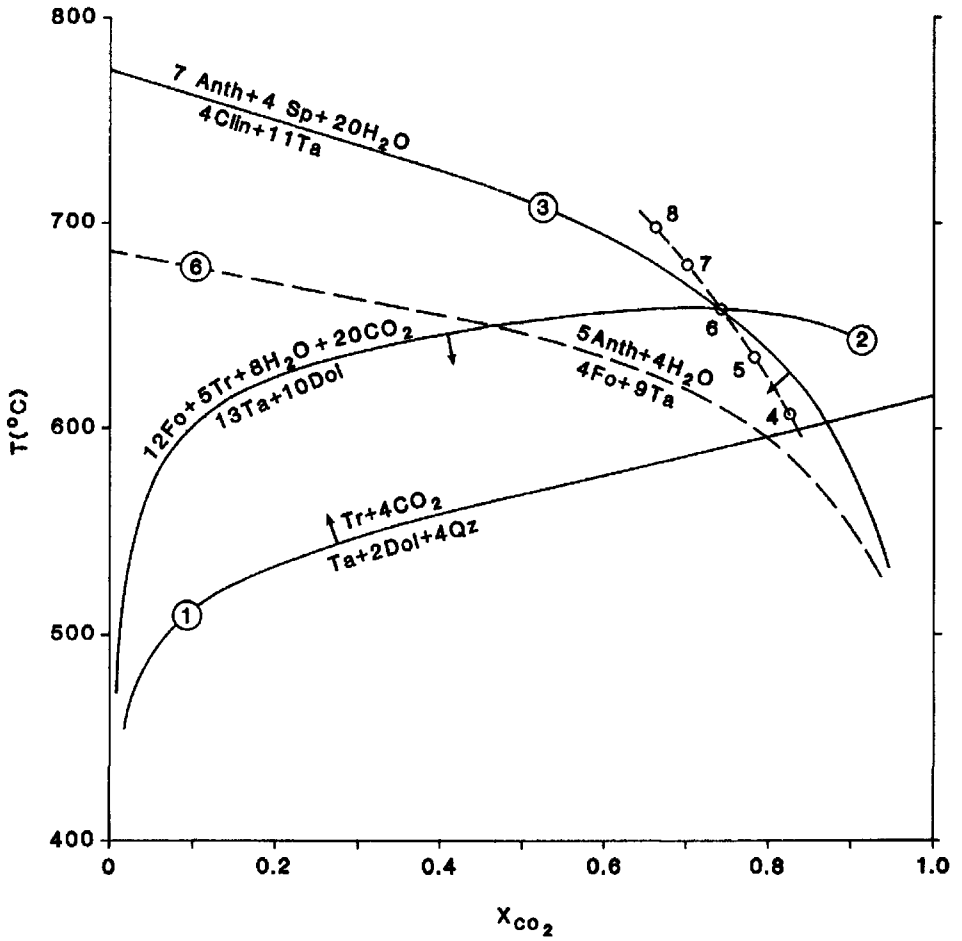

FIG. 6. Stability limits of the assemblage tremolite + talc + chlorite + dolomite + fluid in sample Ach5A, plotted on a T–X_{CO_2} diagram for a pressure of 6 kbar. Numbered curves correspond to equilibria mentioned in the text. Arrows indicate the stable sides of limiting curves. Also shown is the position of the indifferent crossing of curves 2 and 3 (which controls the upper temperature limit of the assemblage) as a function of pressure (values in kbar). Calculated for real mineral compositions using the activity models and thermodynamic data of Holland and Powell (1990). X_{CO_2} = mole fraction of CO_2 in the fluid phase, assuming it to be a binary H_2O–CO_2 mixture.

of intergrowths of up to six of these minerals (e.g. Fig. 1*h*), all of which may be present at the external growth surface of a single compound prism, strongly suggests that their crystallization did not occur under equilibrium conditions. Application of the Gibbs phase rule yields zero degrees of freedom for assemblages in Ach 6B and Ach 9A, assuming the presence of a binary H_2O–CO_2 fluid during metamorphism; as it is extremely unlikely that these assemblages are truly invariant, disequilibrium is implied.

The local correspondence between external morphology (specifically prism zone interfacial angles) and phase identity within compound pyribole prisms indicates that the latter are not simply pseudomorphs after amphibole. The TCP 'wing' regions are clearly overgrowths. The large size and random orientation of the prisms suggests that they grew during prograde metamorphism; supporting this is the observation that, in some samples, the prisms cross-cut a recrystallized chlorite + dolomite schistosity indicating that

they grew during a phase of static metamorphism that post-dated deformation under amphibolite-facies conditions. If the prisms are of Inverian age, as suggested, this implies that the Inverian metamorphism involved some heating. If true, published P–T paths for Scourian metamorphism that portray the Inverian as merely a stage on the retrograde cooling path from the Badcallian granulite-facies thermal peak (e.g. Cartwright and Barnicoat, 1987) must be incorrect.

Pyribole-producing reactions

The disposition of phases within compound prisms indicates, in most cases, that the Mg,Fe-pyriboles present were all crystallizing simultaneously during the late stages of prism growth. The inference is that, within each rock, these phases were all produced by the same fundamental mineral reaction.

Because of the paucity of possible Al-free Mg-rich reactant and product phases in the rocks, the identities of the pyribole-producing reactions are obscure. Several possible closed-system Mg,Fe-continuous reactions exist, all involving one or more 'inferred' reactant minerals:

$$\text{diopside} + \text{enstatite} + H_2O + CO_2 = \text{Mg,Fe-pyribole} + \text{dolomite} \quad (4)$$

$$\text{diopside} + \text{forsterite} + H_2O + CO_2 = \text{Mg,Fe-pyribole} + \text{dolomite} \quad (5)$$

$$\text{talc} + \text{forsterite} = \text{Mg,Fe-pyribole} + H_2O \quad (6)$$

$$\text{Ca-amphibole} + \text{forsterite} + H_2O + CO_2 = \text{Mg,Fe-pyribole} + \text{dolomite} \quad (7)$$

$$\text{Ca-amphibole} + \text{forsterite} + H_2O + CO_2 = \text{Mg,Fe-pyribole} + \text{calcite}. \quad (8)$$

Forsterite, enstatite and diopside are characteristic of Badcallian granulite-facies mineral assemblages in ultramafic rocks (e.g. Sills, 1982) and may have been present in the high-grade precursors of the Achmelvich TCP-bearing rocks. Although chemographically valid, *direct* transformation of pyroxene-bearing assemblages to Mg,Fe-pyribole + carbonate (by e.g. reaction (4) or (5)) would imply straightforward retrogression; this is considered unlikely for reasons given above. More likely would be a reaction involving production of Mg,Fe-pyribole ± carbonate from an amphibolite-facies assemblage of forsterite + hydrous silicate (e.g. (6), (7) or (8)).

No forsterite now exists in any of the samples studied; if it ever did, it must have reacted out completely. Reaction (6) can be invoked for Ach 9A and similar talc-rich samples, but for talc-free samples (e.g. Ach 1A) it would imply that talc and forsterite were exhausted simultaneously, which is improbable. The problem with reactions (7) and (8) is that there is no textural evidence for the consumption of Ca-amphibole. Although the actinolite cores in many compound prisms are irregular (e.g. Fig. 1*a*, *e*) and chemically zoned, the intergrowths with cummingtonite are probably due to co-precipitation or exsolution rather than replacement. Also, once the pyribole-producing reaction had started, the actinolite cores would have become armoured from further reaction with forsterite by the intervening pyribole rims.

Several versions of each of the above reactions can be balanced, depending on the pyribole chosen. The anthophyllite version of (6), for instance, is:

$$4\ Mg_2SiO_4 + 9\ Mg_3Si_4O_{10}(OH)_2 = 5\ Mg_7Si_8O_{22}(OH)_2 + 4\ H_2O. \quad (9)$$

forsterite talc anthophyllite fluid

Thermodynamic calculations (Fig.6) confirm that this reaction proceeds to the right at constant water activity and pressure. However, as the curve has negative dT/dX_{CO_2} (Fig. 6), an influx of CO_2-rich fluid at constant P and T would have the same effect. Although currently untestable by calculation, the jimthompsonite and related versions of reaction (6) are likely to behave in the same way. In reactions (7) and (8), however, pyribole production involves consumption of both H_2O and CO_2 and therefore occurs with decreasing T at constant water activity. At low values of X_{CO_2} such curves are bound to have positive dT/dX_{CO_2} (Kerrick, 1974), so that pyribole production by either of these reactions could also be promoted by an isobaric increase in X_{CO_2} at constant or slightly increasing T, as in the case of (9). This means that, irrespective of the actual reaction involved, pyribole crystallization could have been brought about by infiltration of CO_2-rich fluid during heating.

Pyribole nucleation

The simultaneous crystallization of up to six chemically similar Mg,Fe-pyriboles within a single compound prism must be the result of local variations in nucleation kinetics. In cases where the pyriboles have grown on an actinolite core, it is easy to see why such differences exist. Other things being equal, the surface energy and strain energy terms in the expression for the activation energy of nucleation will be minimized where nucleation is coherent and where there is greatest structural similarity between substrate

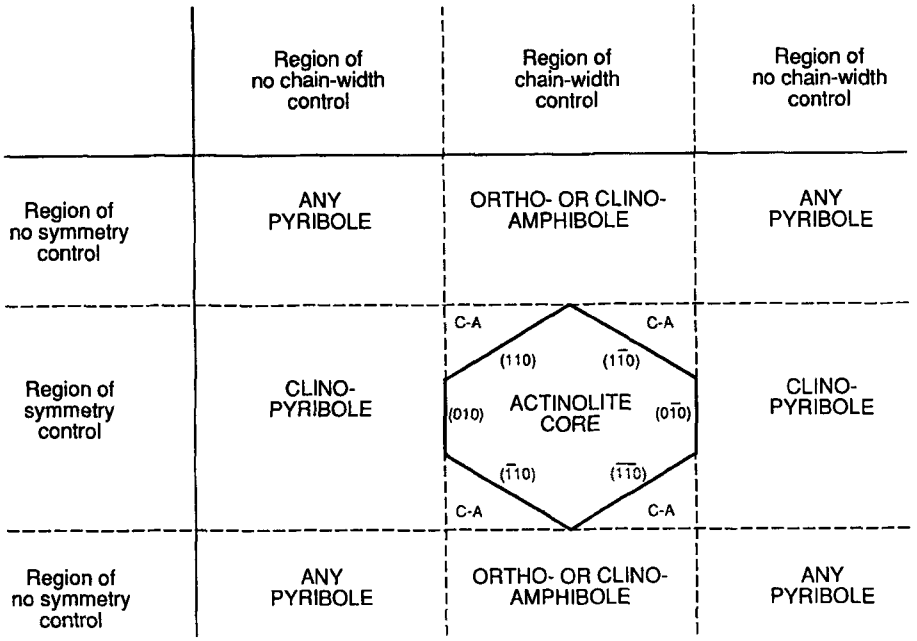

FIG. 7. Schematic diagram to illustrate how the chain width and monoclinic symmetry of an actinolite core are expected to influence the identity of the Mg,Fe-pyriboles nucleating and growing in different parts of a coherent overgrowth. C-A: clino-amphibole. See text for explanation.

and nucleus (e.g. Porter and Easterling, 1981; Worden *et al.*, 1992). Because the layer modules of the generalized pyribole structure are parallel to (010), chain-width is a key feature of the structural 'templates' presented at crystal surfaces at high angles to (010); it follows that nucleation on actinolite {100} or {110} faces will tend to favour pyriboles with the same chain-width, i.e. amphiboles. Nucleation on actinolite {010} faces, on the other hand, will not be controlled by chain width; instead, the key elements of the {010} template will be the *a*-dimension and β angle of the unit cell. The monoclinic nature of the actinolite substrate will tend to favour nucleation of a clino-pyribole on {010}. This is almost universally observed in the Achmelvich samples. Nucleation on the oblique {110} faces of the actinolite will be controlled by both chain-width and symmetry, and will tend to favour clino-amphibole (e.g. cummingtonite), as observed. On an amphibole prism of typical habit (i.e. bounded on a macroscopic scale by {110} and {010} prism forms), the only places where nucleation is likely to be free of symmetry control are the (110)–(1$\bar{1}$0) and ($\bar{1}$10)–($\bar{1}\bar{1}$0) edges plus any incipient {100} faces that may be present along those edges on a microscopic scale.

The same principles may be used to explain how the pyribole domains develop after nucleation. Once an Mg,Fe-pyribole has nucleated, it will continue to grow until either the reaction supplying the necessary components stops or another phase nucleates on it. Nucelation of a second Mg,Fe-pyribole will be subject to the same template controls as that of the first, the only difference being in the identity of the pyribole substrate (Mg,Fe-pyribole *vs.* actinolite). Figure 7 shows how the influences of the chain width and monoclinic symmetry of the actinolite core may be expected to propagate outwards as the pyribole overgrowths continue to crystallize, leading to the development of prism-shaped domains that meet on planes parallel to (010) or (100).

This simple model of template control explains why, in cross-sections of compound pyribole prisms, chain-width type generally appears to be perpetuated parallel to the *a*-axis direction, while symmetry (clino *vs.* ortho) is perpetuated parallel to the *b*-axis direction (Figs. 1*b,e,h*; 2*a,b,c*; 3*a,d*). Exceptions to the former generalization, in particular the rarely observed terminations of (010) lamellae and the more common occurrence of TCP lamellae in cummingtonite-rich overgrowths on actinolite {110} faces, may be

explained with reference to the termination rules of Veblen and Buseck (1980).

Stabilities of triple-chain pyriboles

It is not yet known whether any of the four TCP phases has a stability field on the *P–T* plane, and if so where its limits lie. To date, no equilibria involving TCPs in the $MgO–FeO–SiO_2–H_2O$ system have been located successfully by experiment; in view of the structural disorder commonly encountered in synthetic amphiboles (e.g. Ahn *et al.*, 1991) it is doubtful whether any ever will be. The static energy calculations of Abbott and Burnham (1991) indicate that jimthompsonite and clinojimthompsonite are more stable than their respective equivalent talc + pyroxene and talc + amphibole assemblages at absolute zero, but have little bearing on relative stabilities at geologically realistic conditions. Veblen and Buseck (1979) argued that if TCPs are stable, their stability fields are likely to be very narrow and to lie between those of anthophyllite and talc.

The present observations add little to this debate. The predominance of clinojimthompsonite over jimthompsonite in most (but not all) of the Achmelvich samples is probably governed more by nucleation kinetics than by relative stability; supporting this is the strong correlation between the abundances of clinojimthompsonite and actinolite in different rock samples and in different pyribole prisms within a single sample. However, one piece of circumstantial evidence suggests that jimthompsonite may have been more stable than clinojimthompsonite in the Achmelvich rocks. In almost every compound prism containing both orthorhombic and monoclinic Mg,Fe-pyriboles, the former predominate only where no influence on symmetry could have been exerted by any pre-existing core of actinolite (i.e. only where no actinolite occurs 'along strike' in a direction parallel to the *b*-axis — see Fig. 1). It would thus appear that, once free of substrate control of symmetry, Mg,Fe-pyriboles tended to crystallize preferentially as orthorhombic polytypes, possibly reflecting a closer approach to equilibrium. Carrying this argument further, it would also appear that triple-chain structures were favoured over double-chain ones in regions devoid of substrate control of chain-width (the 'wings'), suggesting that fully triple-chain silicates (MMP structure) were more stable than Mg,Fe-amphiboles during crystallization. This implies that jimthompsonite (the orthorhombic MMP phase) was probably the most stable Mg,Fe-pyribole during the later stages of pyribole crystallization in many of the Achmelvich rocks.

Conclusions

(a) Triple-chain pyriboles occur in amphibolite-facies ultramafic rocks at Achmelvich, NW Scotland, where they form complex intergrowths with one another and with amphiboles in large euhedral compound prisms. Clinojimthompsonite is the most abundant TCP phase, but jimthompsonite and probably chesterite and its monoclinic polytype also occur.

(b) Clinojimthompsonite has the following optical properties: maximum birefringence ($\gamma–\alpha$) = 0.027, extinction angle ($\gamma:c$) = 10°, optic axial plane = (010), and $2V_\alpha$ = 67°.

(c) The TCP phases all have compositions lying essentially within the system $MgO–FeO–SiO_2–H_2O$, with only trace amounts of other components. There is a positive correlation between the Mg/Fe ratios of Mg,Fe-biopyriboles and the proportion of talc (010) layer modules in the structure. Orthorhombic Mg,Fe-pyriboles have slightly higher Mg/Fe ratios than their monoclinic polytypes.

(d) Although substantial volumes of single-phase clinojimthompsonite occur, TCPs and Mg,Fe-amphiboles are locally intergrown on (010) on scales down to 0.1 μm and probably smaller, indicating considerable chain-width disorder.

(e) The TCPs are not pseudomorphous after amphibole and do not appear to be retrogressive. The compound TCP + amphibole prisms resemble prograde porphyroblasts. The Inverian metamorphism, in which these minerals grew, was probably not simply a late retrograde phase of the Scourian granulite-facies metamorphism but involved some heating.

(f) The TCP phases formed at temperatures less than 600–700°C by reactions that probably involved breakdown of olivine. Infiltration of CO_2-rich fluid may have promoted these reactions.

(g) The observed TCP assemblages do not represent equilibrium associations; rather, they are a function of nucleation kinetics. The disposition of TCP phases within compound prisms may be explained, at least in general, by 'template'-controlled nucleation.

(h) Despite the predominance of its monoclinic polytype, jimthompsonite was probably the most stable Mg,Fe-pyribole phase during the later stages of pyribole growth in the Achmelvich rocks.

Acknowledgements

I am indebted to Graham Chinner for drawing my attention to triple-chain silicates. This work has also benefited from discussions with Kate Brodie,

Pam Champness, Maryla Dorling, Geoff Lloyd, Simon Redfern, John Schumacher, Dave Waters and Jack Zussman. Thanks go to Dave Plant, Tim Hopkins, Brian Smith and Steve Caldwell for technical assistance. Constructive reviews by Mark Welch and Jim Chisholm are gratefully acknowledged.

References

Abbott, R. N. and Burnham, C. W. (1991) Energy calculations bearing on biopyriboles. *Amer. Mineral.*, **76**, 728–32.

Ahn, J. H., Cho, M., Jenkins, D. M. and Buseck, P. R. (1991) Structural defects in synthetic tremolitic amphiboles. *Amer. Mineral.*, **76**, 1811–23.

Akai, J. (1982) Polymerization process of biopyribole in metasomatism at the Atakani ore deposit, Japan. *Contrib. Mineral. Petrol.*, **80**, 117–31.

Cartwright, I. and Barnicoat, A. C. (1986) The generation of silica-undersaturated melts and corundum-bearing restites by crustal anatexis: petrogrenetic modelling based on an example from the Lewisian of NW Scotland. *J. Metamorph. Geol.*, **4**, 79–100.

Cartwright, I. and Barnicoat, A. C. (1987) Perology of Scourian supracrustal rocks and orthogneisses from Stoer, N.W. Scotland: implications for the geological evolution of the Lewisian Complex. In *Evolution of the Lewisian and comparable Precambrian high grade terrains* (Park, R. G. and Tarney, J., eds.) *Geol. Soc. Special Publ.*, **27**, 93–107.

Chapman, H. J. (1979) 2390 Myr Rb–Sr whole-rock age for the Scourie Dykes of north-west Scotland. *Nature*, **277**, 642–3.

Chapman, H. J. and Moorbath, S. (1977) Lead isotope measurements from the oldest recognised Lewisian gneisses of north-west Scotland. *Nature*, **268**, 41–2.

Cressey, B. A., Whittaker, E. J., and Hutchison, J. L. (1980) Electron microscopy of amphiboles along [001]. *Abstracts, I.M.A. 12th General Meeting, Orleans*, p. 94 (abstract).

Deer, W. A., Howie, R. A., and Zussman, J. (1992) *Introduction to the rock-forming minerals.* (Second Edition) Longman, London.

Dorling, M. and Zussman, J. (1984) Zincian actinolite asbestos. *Mineral. Pol.*, **15**, 11–20.

Drits, V. A., Goncharov, Y. I., Aleksandrova, V. A., Khadzhi, V. E., and Dmitrik, A. L. (1974) A new type of strip silicate. *Kristallografiya*, **19**, 1186–93.

Evans, C. R. (1965) Geochronology of the Lewisian basement near Lochinver, Sutherland. *Nature*, **207**, 54–6.

Evans, C. R. and Lambert, R. St. J. (1974) The Lewisian of Lochinver, Sutherland; the type area for the Inverian metamorphism. *J. Geol. Soc.*, **130**, 125–50.

Evans, C. R. and Tarney, J. (1964) Isotopic ages of Assynt dykes. *Nature*, **205**, 638–41.

Hamilton, P. J., Evensen, N. M., O'Nions, R. K., and Tarney, J. (1979) Sm-Nd systematics of Lewisian gneisses: implications for the origin of granulites. *Nature*, **277**, 25–8.

Holland, T. J. B. and Powell, R. (1990) An enlarged and updated internally consistent thermodynamic dataset with uncertainties and correlations: the system K_2O-Na_2O-CaO-MgO-MnO-FeO-Fe_2O_3-Al_2O_3-TiO_2-SiO_2-C-H_2-O_2. *J. Metamorph. Geol.*, **8**, 89–124.

Humphries, F. J. and Cliff, R. A. (1982) Sm-Nd dating and cooling history of Scourian ganulites, Sutherland. *Nature*, **295**, 515–7.

Kerrick, D. M. (1974) Review of metamorphic mixed-volatile (H_2O-CO_2) equilibria. *Amer. Mineral.*, **59**, 729–62.

Livi, K. J. T. and Veblen, D. R. (1992) An analytical electron microscopy study of pyroxene-to-pyroxenoid reactions. *Amer. Mineral.*, **77**, 380–90.

Lloyd, G. E. (1987) Atomic number and crystallographic contrast images with the SEM: a review of backscattered electron techniques. *Mineral. Mag.*, **51**, 3–19.

Moorbath, S., Powell, J. L. and Taylor, P. N. (1975) Isotopic evidence for the age and origin of the 'grey gneiss' complex of the southern Outer Hebrides, Scotland. *J. Geol. Soc. London*, **131**, 213–22.

Nakajima, Y. and Ribbe, P. H. (1980) Alteration of pyroxenes from Hokkaido, Japan, to amphiboles, clays and other biopyriboles. *Neues Jahrb. Mineral., Mh.*, 258–68.

Nissen, H.-U., Wessicken, R., Woensdregt, C. F. and Pfeifer, H. R. (1979) Disordered intermediates between jimthompsonite and anthophyllite from the Swiss Alps. In *Electron microscopy and analysis 1979* (Mulvey, T., ed.) *Institute of Physics, Conference Series*, **52**, 99–100.

Park, R. G. and Tarney, J. (1987) The Lewisian Complex. In *Evolution of the Lewisian and comparable Precambrian high grade terrains* (Park, R.G. and Tarney, J., eds.) *Geol. Soc. Special Publ.*, **27**, 13–25.

Pidgeon, R. T. and Bowes, D. R. (1968) Zircon U–Pb ages of granulites from the central region of the Lewisian, north-west Scotland. *Geol. Mag.*, **109**, 247–58.

Porter, D. A. and Easterling, K. E. (1981) *Phase transformations in metals and alloys.* Van Nostrand Reinhold (UK), Wokingham.

Ross, M., Papike, J. J. and Shaw, K. W. (1969) Exsolution textures in amphiboles as indicators of subsolidus thermal histories. *Mineral. Soc. Am.*

Special Paper, **2**, 275–99.

Schumacher, J. C. and Czank, M. (1987) Mineralogy of triple- and double-chain pyriboles from Orijärvi, southwest Finland. *Amer. Mineral.*, **72**, 345–52.

Sheraton, J. W., Tarney, J., Wheatley, T. J. and Wright, A. E. (1973) The structural history of the Assynt district. In *The early Precambrian of Scotland and related rocks of Greenland* (Park, R. G. and Tarney, J., eds.) Keele, 9–12.

Sills, J. D. (1982) The retrogression of ultramafic granulites from the Scourian of NW Scotland. *Mineral. Mag.*, **46**, 55–61.

Sills, J. D. (1983) Mineralogical changes occurring during the retrogression of Archaean gneisses from the Lewisian complex of NW Scotland. *Lithos*, **16**, 113–24.

Sutton, J. and Watson, J. (1951) The pre-Torridonian metamorphic history of the Loch Torridon and Scourie areas in the north-west Highlands, and its bearing on the chronological history of the Lewisian. *Q. J. Geol. Soc. London*, **106**, 241–308.

Tarney, J. (1978) Achmelvich Bay, Assynt (Lewisian). In *The Lewisian and Torridonian rocks of north-west Scotland* (Barber, A. J., Beach, A., Park, R. G., Tarney, J. and Stewart, A. D. eds.) *Geol. Assoc. Guide*, **21**, 35–50.

Tateyama, H., Shimoda, S., and Sudo, T. (1978) Synthesis and crystal structure of a triple-chain silicate, $Na_2Mg_4Si_6O_{16}(OH)_2$. *Contrib. Mineral. Petrol.*, **66**, 149–56.

Thompson, J. B. (1970) Geometrical possibilities for amphibole structures: model biopyriboles. *Amer. Mineral.*, **55**, 292–3.

Thompson, J. B. (1978) Biopyriboles and polysomatic series. *Amer. Mineral.*, **63**, 239–49.

Treloar, P. J. and Putnis, A. (1982) Chemistry and microstructure of orthoamphiboles from cordierite-amphibole rocks at Outokumpu, North Karelia, Finland. *Mineral. Mag.*, **45**, 55–62.

Veblen, D. R. and Burnham, C. W. (1975) Triple-chain biopyriboles: newly discovered intermediate products of the retrograde anthophyllite-talc transformation. *Trans. Amer. Geophys. Union (EOS)*, **56**, 1076 (abstract).

Veblen, D. R. and Burnham, C. W. (1976) Biopyriboles from Chester, Vermont: the first mixed-chain silicates. *Geol. Soc. Am. Abstracts with Programs*, **8**, 1153 (abstract).

Veblen, D. R. and Burnham, C. W. (1978a) New biopyriboles from Chester, Vermont: I Descriptive mineralogy. *Amer. Mineral.*, **63**, 1000–9.

Veblen, D. R. and Burnham, C. W. (1978b) New biopyriboles from Chester, Vermont: II The crystal structures of jimthompsonite, clino-jimthompsonite and chesterite, and the amphibole-mica reaction. *Amer. Mineral.*, **63**, 1053–73.

Veblen, D. R. and Buseck, P. R. (1979) Chain width order and disorder in biopyriboles. *Amer. Mineral.*, **64**, 687–700.

Veblen, D. R. and Buseck, P. R. (1980) Microstructures and reaction mechanisms in biopyriboles. *Amer. Mineral.*, **65**, 599–623.

Veblen, D. R. and Buseck, P. R. (1981) Hydrous pyriboles and sheet silicates in pyroxenes and uralites: intergrowth microstructures and reaction mechanisms. *Amer. Mineral.*, **66**, 1107–34.

Welch, M. D., Rocha, J., and Klinowski, J. (1992) Characterisation of polysomatism in biopyriboles: double-/triple-chain lamellar intergrowths. *Phys. Chem. Minerals*, **18**, 460–8.

Whittaker, E. J., Cressey, B. A. and Hutchison, J. L. (1981) Terminations of multiple chain lamellae in grunerite asbestos. *Mineral. Mag.*, **44**, 27–35.

Worden, R. H., Droop, G. T. R. and Champness, P. E. (1992) The influence of crystallography and kinetics on phengite breakdown reactions in a low-pressure metamorphic aureole. *Contrib. Mineral. Petrol.*, **110**, 329–45.

Yau, Y-C. and Peacor, D. R. (1985) Wide-chain Ca-pyribole and actinolite intergrowths in primary euhedral crystals from the Salton Sea geothermal field, California. *Trans. Amer. Geophys. Union (EOS)*, **66**, 373 (abstract).

[*Manuscript received 4 December 1992; revised 4 June 1993*]